Supporting information for

# NADH photoregeneration in a fully automated microfluidic setup

*Alberto Bianco,*[a] *Alexander McMillan,*[b] *Carlo Giansante,*[c] *and Giacomo Bergamini**[a]

[a] Dipartimento di Chimica "Giacomo Ciamician", Alma Mater Studiorum – Università di Bologna, Via Selmi 2, 40126 Bologna, Italy

[b] Microfluidics Innovation Center, 172 Rue de Charonne, 75011, Paris, France

[c] Consiglio Nazionale delle Ricerche, Istituto di Nanotecnologia − CNR NANOTEC, Via Monteroni, 73100 Lecce, Italy

Corresponding author's e-mail address: giacomo.bergamini@unibo.it

CHEMICALS

β-Nicotinamide adenine dinucleotide hydrate ($NAD^+$, grade I, free acid, product code 10127965001), reduced β-Nicotinamide adenine dinucleotide hydrate (1,4-NADH, grade I, disodium salt, product code 10107735001) were purchased from Roche Diagnostic GmbH and used as received. High-purity triethanolamine (TEOA, ≥ 99.0%), fuming hydrochloric acid (37% wt) and sodium hydroxide (≥ 99.9%) were purchased from Merck and used with no further purification. $N_2$ and $O_2$ used as carrier gas (filtered on Drierite™, 99.999% purity) were supplied by SIAD. Type 1 ultrapure water was obtained with an Elga PURELAB® Classic UV apparatus.

PHOTOELECTROCHEMICAL CHARACTERIZATION

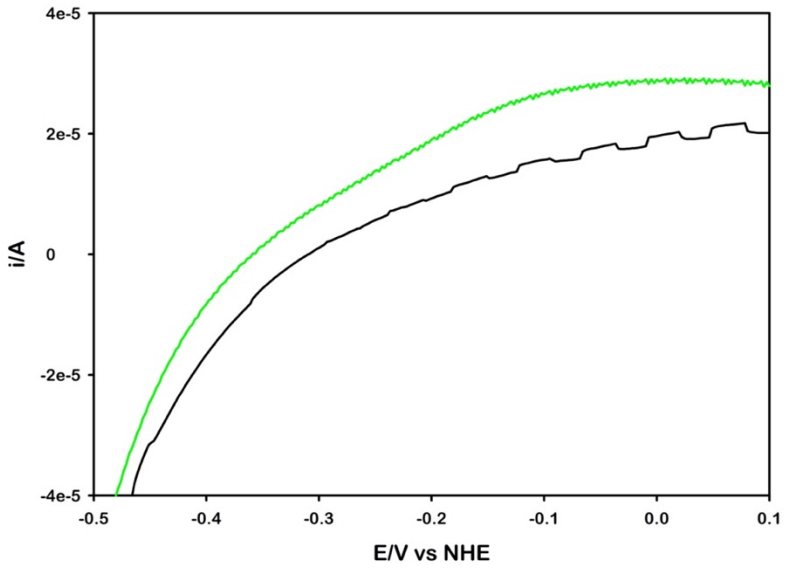


**Figure S1.** LSV experiments (scan rate 10 $mV \cdot s^{-1}$) on $Bi_{13}S_{18}Br_2$ nanocrystals film under chopped light illumination (f = 0.3 Hz) without (green line) and with 0.1 M TEOA addition (black line).

In Figure S1 is clearly evident the effect of TEOA, from the addition of which a photocurrent (both anodic and cathodic) is generated. The effect of chopped light was also investigated, as reported in Figure S2.

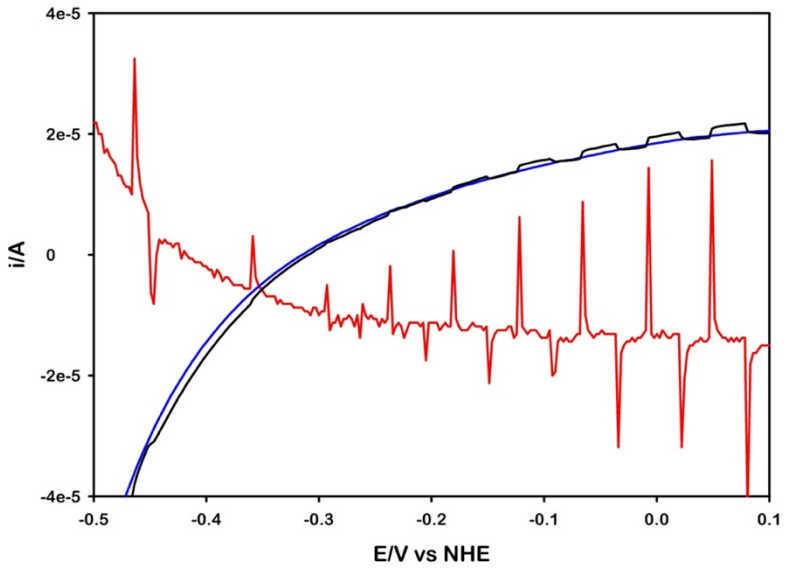


**Figure S2.** LSV experiments (scan rate 10 mV·s-1) on $Bi_{13}S_{18}Br_2$ nanocrystals film with 0.1 M TEOA under chopped light illumination (f = 0.3 Hz; black line) and in the dark (blue line). Red curve represents the first derivative of chopped light LSV.

From this latter measurement it is possible to assess that the flat band potential of the material is located at -0.3 V vs NHE.[1]

THIN FILM CHARACTERIZATION

The AFM images of the nanocrystal thin films, prepared as described in the main text on mica support, were characterized acquired on a Bruker Multimode 8 AFM Nanoscope equipped with a SCANASYST-AIR-HR probe operating in tapping mode. The images were analysed with a mono-dimensional autocorrelation function (ACF) with Gwyddion 2.65, obtaining the results reported in Table S1.

**Table S1.** Geometrical parameter obtained with mono-dimensional ACF analysis on Figure 2b.

| ACF on $Bi_{13}S_{18}Br_2$ film | |
|---|---|
| Roughness | (15 ± 3) nm |
| Height distribution | (99.2 ± 0.1) nm |
| σ | 20 nm |

IRRADIATION SETUP AND OPTIMIZATION

The irradiation setup used in all the experiments is composed by a commercial 460 nm blue LED strip spirally arranged in a shielded plastic cylinder equipped with a fan to ensure cooling of the reaction environment. The conical tube containing the reaction mixture and the nanocrystal film was placed inside the cylinder through a hole in the centre of the lid.

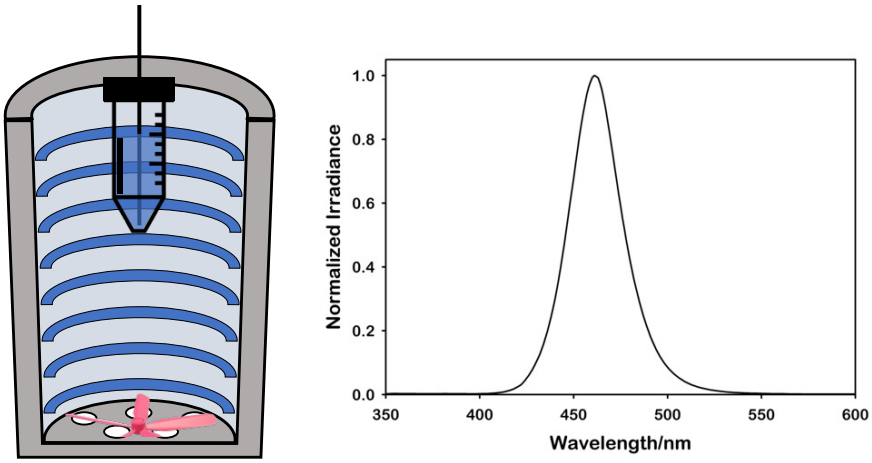


**Figure S3.** Schematic representation of the irradiation setup (left side) and blue LED strip spectral profile (right side).

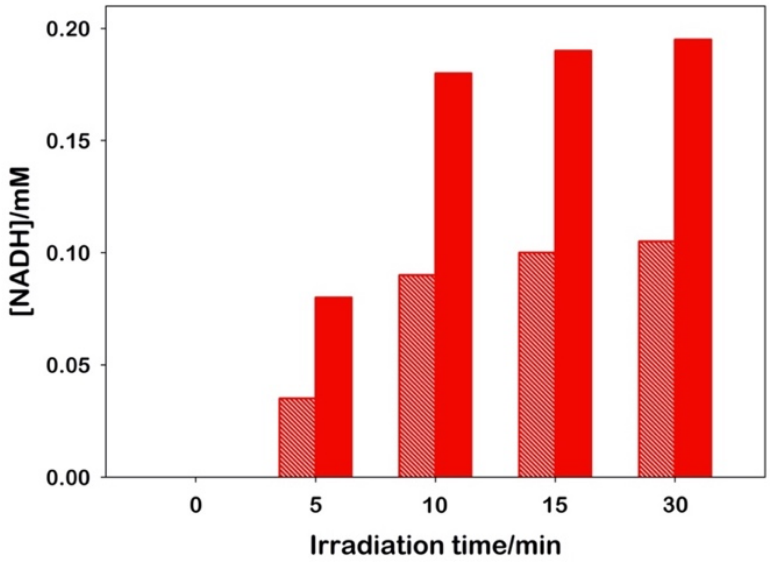


**Figure S4.** Regenerated NADH concentration obtained irradiating the TEOA solution for different durations in oxygen saturated batch (dashed columns) and in microbubble generation system (solid columns).

NAD$^+$ TITRATION

Since the adenine moiety of NAD$^+$ exhibit multiple sites with acid-base activity,[2] we recorded the absorption spectrum of a 2 mM aqueous solution of NAD$^+$ in order to monitor the spectral changes ascribable to these phenomena. The titration was conducted, firstly, in pure water and, secondary, in 0.1 M TEOA solution, without observing any noticeable difference between these two environments.

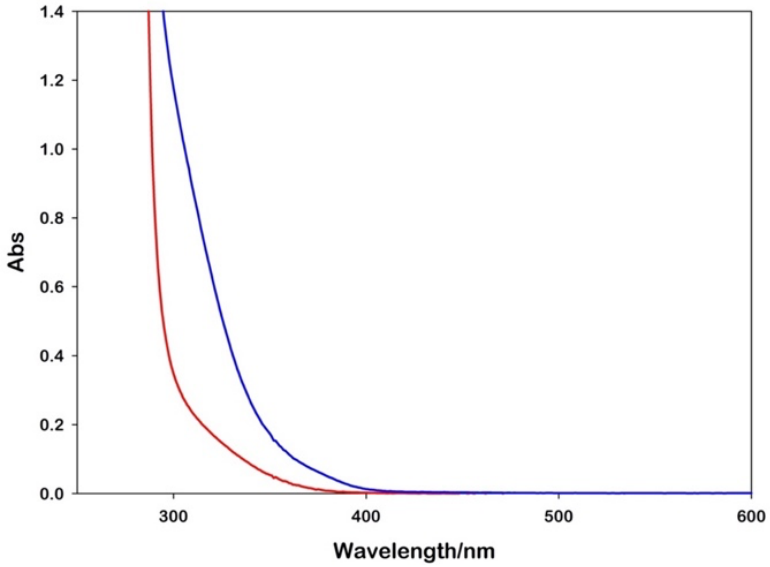


**Figure S5.** Absorption spectra of 2 mM NAD$^+$ aqueous solution at pH = 7.4 (red line) and at pH = 10.5 (blue line).

From this measurement, knowing the molar absorption coefficient of NAD$^+$,[3] it was possible to determine the coefficient of the deprotonated form of NAD$^+$, which then interconverts into NADH.

**Table S2.** Molar absorption coefficients of the species involved in this work.

| | NAD$^+$ | NAD$^+_{pH = 10.5}$ | NADH |
|---|---|---|---|
| $\varepsilon_{340\ nm}$ / $M^{-1} \cdot cm^{-1}$ | 40 | 130 | 6220 |

NADH CONCENTRATION CALCULATION

According to the Beer-Bouguer-Lambert Law, the absorbance of a solution containing a chromophore at a specific wavelength $A_\lambda$ is defined as:

$$A_\lambda = \varepsilon_\lambda \cdot b \cdot C$$

where $\varepsilon_\lambda$ is the molar absorption coefficient of the chromophore in the specific solvent at a $\lambda$ wavelength, $b$ is the optical path length and $C$ is the chromophore molar concentration.

In case of multiple absorbing species in solution, the total absorbance at a specific wavelength is defined as the sum of the absorbance of the single components:

$$A_\lambda = \sum \varepsilon_{\lambda,n} \cdot b \cdot C_n$$

In case of two absorbing species, the above equation can be rewritten as:

$$A_\lambda = \varepsilon_{\lambda,x} \cdot b \cdot C_x + \varepsilon_{\lambda,y} \cdot b \cdot C_y$$

When the $x$ specie is converted into the $y$ specie, following a $x \rightarrow y$ process, the final absorbance is defined as:

$$A_\lambda = \varepsilon_{\lambda,x} \cdot b \cdot (C_x - \Delta C) + \varepsilon_{\lambda,y} \cdot b \cdot (C_y + \Delta C)$$

So, the absorbance variation $\Delta A_\lambda$ can be written as:

$$\Delta A_\lambda = \varepsilon_{\lambda,x} \cdot b \cdot (-\Delta C) + \varepsilon_{\lambda,y} \cdot b \cdot (+\Delta C)$$

Where ΔC is the variation of the molar concentration of the species after the conversion. The latter equation can be rewritten as:

$$\Delta A_\lambda = \Delta \varepsilon_\lambda \cdot b \cdot \Delta C$$

Where $\Delta \varepsilon_\lambda$ is the variation of the molar absorption coefficient between x and y species at a specific wavelength.

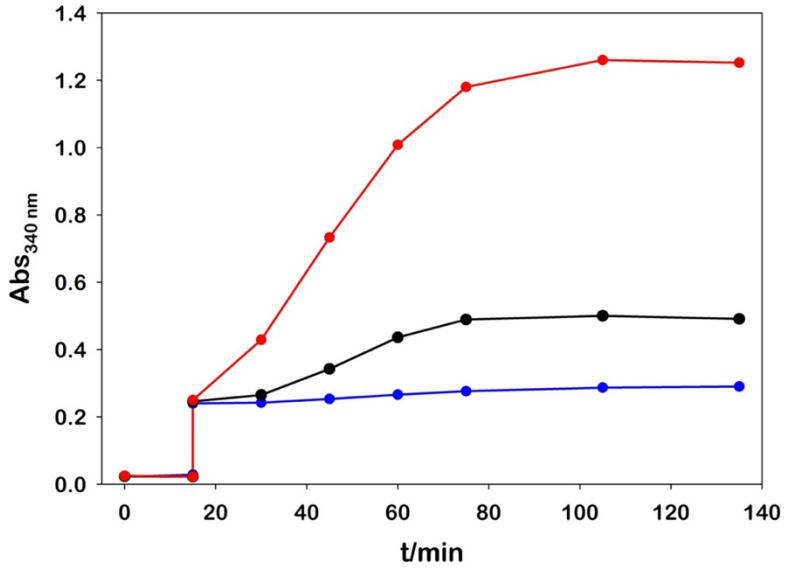


**Figure S6.** 340 nm absorbance variations obtained during NADH regeneration with $N_2$ (blue), air (black) and $O_2$ (red) microbubbles.

CONTROL EXPERIMENTS

The system was tested in automated $O_2$ microbubble setup by omitting one of the components at a time, obtaining the following results:

**Table S3.** Absorbance at 340 nm and 470 nm emission signal obtained after an $O_2$ bubble generation automated cycle in different conditions.

| NC Film | Light | TEOA 0.1 M | $NAD^+$ 2 mM | pH = 10.5 | [NADH]/mM | $Em_{470\ nm}$ |
|---|---|---|---|---|---|---|
| Yes | Yes | Yes | Yes | Yes | 0.18 | Yes |
| No | Yes | Yes | Yes | Yes | 0 | No |
| Yes | No | Yes | Yes | Yes | 0 | No |
| Yes | Yes | No | Yes | Yes | 0 | No |
| Yes | Yes | Yes | No | Yes | 0 | No |
| Yes | Yes | Yes | Yes | No | 0 | No |

**Table S4.** Comparison of mediator-free photocatalytic NADH regeneration systems.

| No. | Photocatalyst | Mass/mg | Light source | TEOA | $[NAD^+]$/mM | Volume/mL | [NADH]/mM | Time/min | Productivity/mmol·$g^{-1}$·$h^{-1}$ | Ref. |
|---|---|---|---|---|---|---|---|---|---|---|
| 1 | NK-COF | 3 | 300 W Xe lamp<br>λ > 420 nm | 300 μL | 1.0 | 3 | 0.60 | 60 | 0.60 | 4 |
| 2 | T-COF-2 | 3 | 300 W Xe lamp<br>λ > 420 nm | 2.01 mM | 1.0 | 3 | 0.44 | 10 | 2.63 | 5 |
| 3 | PDI/CN | 10 | AM 1.5 | 15 % wt | 1.0 | 10 | 0.45 | 180 | 0.15 | 6 |
| 4 | TCM-15% | 15 | 300 W Xe lamp<br>λ > 420 nm | 15 % w/V | 1.0 | 10 | 0.45 | 30 | 0.92 | 7 |
| 5 | $Bi_{13}S_{18}Br_2$ | 0.05 | Blue LED strip<br>λ = 450 nm | 0.1 M | 2.0 | 3 | 0.18 | 40 | 16.2 | This work |

REFERENCES

(1) Hankin, A.; Bedoya-Lora, F. E.; Alexander, J. C.; Regoutz, A.; Kelsall, G. H. Flat Band Potential Determination: Avoiding the Pitfalls. *J. Mater. Chem. A* **2019**, *7* (45), 26162–26176. https://doi.org/10.1039/C9TA09569A.

(2) Nguyen, M. T.; Uchimaru, T.; Zeegers-Huyskens, T. Protonation and Deprotonation Enthalpies of Guanine and Adenine and Implications for the Structure and Energy of Their Complexes with Water: Comparison with Uracil, Thymine, and Cytosine. *J. Phys. Chem. A* **1999**, *103* (44), 8853–8860. https://doi.org/10.1021/jp990647+.

(3) Bernofsky, C.; Wanda, S. Y. Formation of Reduced Nicotinamide Adenine Dinucleotide Peroxide. *J. Biol. Chem.* **1982**, *257* (12), 6809–6817. https://doi.org/https://doi.org/10.1016/S0021-9258(18)34502-2.

(4) Zhao, Z.; Zheng, D.; Guo, M.; Yu, J.; Zhang, S.; Zhang, Z.; Chen, Y. Engineering Olefin-Linked Covalent Organic Frameworks for Photoenzymatic Reduction of CO2. *Angew. Chemie Int. Ed.* **2022**, *61* (12), e202200261. https://doi.org/https://doi.org/10.1002/anie.202200261.

(5) Wang, Y.; Liu, H.; Pan, Q.; Wu, C.; Hao, W.; Xu, J.; Chen, R.; Liu, J.; Li, Z.; Zhao, Y. Construction of Fully Conjugated Covalent Organic Frameworks via Facile Linkage Conversion for Efficient Photoenzymatic Catalysis. *J. Am. Chem. Soc.* **2020**, *142* (13), 5958–5963. https://doi.org/10.1021/jacs.0c00923.

(6) Zhang, P.; Hu, J.; Shen, Y.; Yang, X.; Qu, J.; Du, F.; Sun, W.; Li, C. M. Photoenzymatic Catalytic Cascade System of a Pyromellitic Diimide/g-C3N4 Heterojunction to Efficiently Regenerate NADH for Highly Selective CO2 Reduction toward Formic Acid. *ACS Appl. Mater. Interfaces* **2021**, *13* (39), 46650–46658. https://doi.org/10.1021/acsami.1c13167.

(7) Wei, P.; Dong, J.; Gao, X.; Chang, L.; Huang, Z.; Zheng, H.; Lee, S. M.-Y.; Lou, W.-Y.; Peng, C. Efficient NADH Regeneration without Electron Mediator toward Enzymatic CO2 Reduction

Enabled by a Lawn-like TP-COFs/Ti3C2Tx (MXene) Photocatalyst. *ACS Sustain. Chem. Eng.* **2024**, *12* (18), 6881–6893. https://doi.org/10.1021/acssuschemeng.3c07466.